JACS
JOURNAL OF THE AMERICAN CHEMICAL SOCIETY

COMMUNICATION

pubs.acs.org/JACS

Hydrodynamic Fractionation of Finite Size Gold Nanoparticle Clusters

De-Hao Tsai,[†] Tae Joon Cho,[†] Frank W. DelRio,[†] Julian Taurozzi,[†] Michael R. Zachariah,[†,‡] and Vincent A. Hackley*[,†]

[†]Material Measurement Laboratory, National Institute of Standards and Technology, Gaithersburg, Maryland 20899, United States

[‡]Departments of Mechanical Engineering and Chemistry, University of Maryland, College Park, Maryland 20740, United States

Supporting Information

ABSTRACT: We demonstrate a high-resolution in situ experimental method for performing simultaneous size classification and characterization of functional gold nanoparticle clusters (GNCs) based on asymmetric-flow field flow fractionation (AFFF). Field emission scanning electron microscopy, atomic force microscopy, multi-angle light scattering (MALS), and in situ ultraviolet−visible optical spectroscopy provide complementary data and imagery confirming the cluster state (e.g., dimer, trimer, tetramer), packing structure, and purity of fractionated populations. An orthogonal analysis of GNC size distributions is obtained using electrospray-differential mobility analysis (ES-DMA). We find a linear correlation between the normalized MALS intensity (measured during AFFF elution) and the corresponding number concentration (measured by ES-DMA), establishing the capacity for AFFF to quantify the absolute number concentration of GNCs. The results and corresponding methodology summarized here provide the proof of concept for general applications involving the formation, isolation, and in situ analysis of both functional and adventitious nanoparticle clusters of finite size.

Gold nanoparticle clusters (GNCs) with controlled size and functionality are attractive for a variety of applications in nanotechnology,[1−5] including the rational fabrication of nanoscale devices.[5] Their functional response is effectively determined by their physical properties, including primary particle and cluster dimensions as well as interparticle spacing and orientation.[2−4,6] Moreover, the presence of adventitious GNCs in an otherwise singlet gold nanoparticle population can prove detrimental for critical applications such as nanomedicine, where size is highly determinant with respect to efficacy and other factors.[7−9] Hence, the ability to detect, control, and assess the physical/dimensional properties of GNCs in situ is vitally important.

Molecular conjugation is frequently utilized as a method to provide control over physical properties during cluster formation;[10] however, without further size classification, the homogeneity of these functionalized GNCs is typically less than ideal (i.e., the heterodispersity problem). Furthermore, the formation and isolation of finite size small clusters by solution-phase methods is extremely challenging due to the dynamic and unstable nature of these systems. In previous publications, Chen and co-workers[2,3] have demonstrated that density gradient centrifugation can yield well-separated bands highly enriched with GNC dimers or trimers, a substantial improvement with respect to GNC purity.

In the present study, we demonstrate a hydrodynamic fractionation approach based on asymmetric-flow field flow fractionation (AFFF), which enables well-resolved separation of purified GNC fractions (comparable in purity to density gradient centrifugation) with simultaneous in situ characterization of GNC size distribution and optical properties.[11] The separation principle is based on the balance of forces between an applied cross-flow (transverse fluid flow relative to the direction of elution) and random particle diffusion; this balance leads to rapid separation based on hydrodynamic size (see Supporting Information for details). Moreover, the eluting fractionated bands can be collected and analyzed off-line or ex situ for further confirmation of properties. The capacity of AFFF to fractionate singlet gold nanoparticles (AuNPs) from mixed size populations has been demonstrated previously for relatively monodisperse source materials,[12] but the challenge is much greater for cluster separation due to the broader range of possible subpopulations and the smaller dimensional ratios involved.

Our principal objective here was to obtain high-purity GNCs with simultaneous and orthogonal characterization for quality assurance. To reach this objective, we utilized several online and off-line methods in addition to, or in conjunction with, AFFF. Our customized AFFF system includes two online detectors: a diode array detector provides full spectral analysis in real time based on ultraviolet−visible (UV−vis) optical spectroscopy, and a multi-angle light scattering (MALS) detector provides angular-resolved optical scattering profiles for eluting bands. Atomic force microscopy (AFM) and field emission scanning electron microscopy (FE-SEM) provide imagery of GNCs sampled from the eluting bands. Finally, these results are cross-related with electrospray-differential mobility analysis (ES-DMA), which provides high-resolution particle size classification of unfractionated aerosolized GNCs for orthogonal comparison with AFFF and for normalization of MALS data.

Cluster formation was induced via the controlled addition of ammonium acetate as an electrostatic screening agent: as the repulsive surface charge is increasingly screened, attractive van der Waals forces dominate and increase the likelihood of binding during collision events.[6] Figure 1a shows the particle size distributions obtained from AFFF fractograms for cluster formation in nominally 10 and 30 nm AuNP suspensions, denoted as 10-GNC and 30-GNC, respectively. In both cases, at least five distinct

Received: April 21, 2011
Published: May 16, 2011

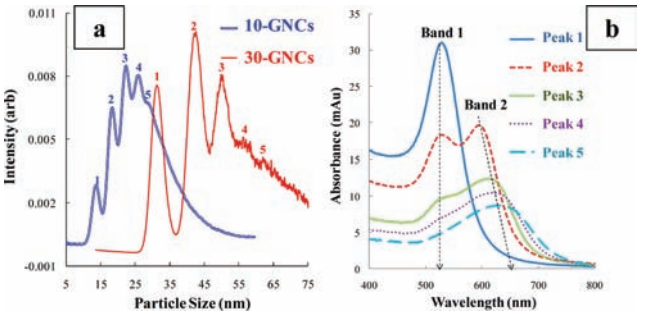

Figure 1. Characterization of GNCs by AFFF. (a) Particle size distribution of 10-GNCs and 30-GNCs. (b) In situ UV−vis spectra for 30-GNCs from peak 1 to peak 5 shown in panel a.

peaks can be resolved, presumably due to the formation of GNCs having different values of n, where n is the finite number of primary AuNPs per cluster.[6] In situ UV−vis (see Figure 1b for 30-GNC as an example) shows that the primary surface plasmon resonance (SPR) band decreases in magnitude, while a secondary (longitudinal) band (at $\lambda_{2,max}$) appears and then red-shifts as the characteristic peak size increases (e.g., $\lambda_{2,max}$ shifts from 588 to 628 nm, corresponding to an increase in n from peak 2 to peak 5). The decrease in frequency associated with the longitudinal SPR[2] confirms the increase of cluster size (i.e., the increase of n effectively increases the aspect ratio of GNCs, thereby red-shifting the longitudinal SPR, a phenomenon similar to that observed for high-aspect Au nanorods and nanowires).[13]

FE-SEM visualization of GNCs collected after fractionation by AFFF confirms peak assignments with respect to the cluster number. For visual clarity, we include here only images for 30-GNCs. Figure 2a (using the fraction of peak 2 in Figure 1a as an example) shows that deposition is homogeneous on the substrate and that deposited particles are well spaced and therefore less subject to artifacts (FE-SEM images for the other 30-GNCs fractions are given in the Supporting Information). Histograms based on analysis of FE-SEM images (Figure 2b; at least 150 particles are counted per fraction) identify the dominant cluster species for each AFFF peak as follows: monomer in peak 1 [(90 ± 1)%], dimer in peak 2 [(86 ± 2)%], trimer in peak 3 [(62 ± 3)%], tetramer in peak 4 [(36 ± 3)%], and pentamer in peak 5 [(36 ± 4)%]. Estimated uncertainties are calculated on the basis of one standard deviation of the total particle count.[14] Overall, the results confirm our assignment of characteristic cluster numbers to specific fractogram peaks for $n < 6$, and clearly demonstrate the capacity for AFFF to resolve small GNCs into highly enriched bands. We believe that these results can be further improved by optimization of AFFF parameters, including flow rates, injection volume, membrane type, pore size, and channel depth; however, our principal intent here is to communicate proof of concept and not to optimize the process.

The purity of GNCs within fractionated bands obtained by AFFF is comparable to that obtained previously by Chen et al.[2] using density gradient centrifugation (up to 85% purity in the dimer band and 70% purity in the trimer band after the first pass). Moreover, the AFFF method offers three additional benefits: (1) GNCs are obtained in their native medium (~0.02% mass ratio of inorganic salts in deionized water in the present case) without the requirement for further purification to remove high levels of salt required to create a density gradient; (2) polymeric capping agents are not required to facilitate separation by AFFF; and (3) GNC

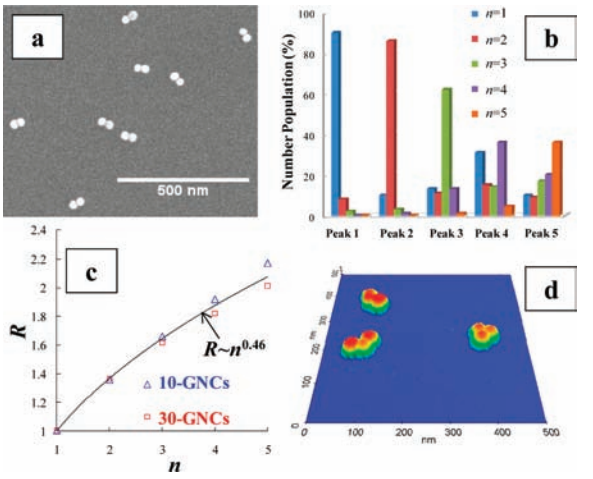

Figure 2. FE-SEM and AFM analysis of 30-GNCs fractions resolved by AFFF. (a) FE-SEM image of peak 2 fraction in Figure 1a. Scale bar is 500 nm. (b) Histograms generated from FE-SEM images. (c) R vs n measured in Figure 1a. Curve is the power law fit to triangles and squares representing experimental data of 10-GNCs and 30-GNCs, respectively. (d) AFM image of peak 3 fraction in Figure 1a. The height (z direction) scale is from 0 to 30 nm.

cluster size and number, as well as characteristic optical properties, can be measured in situ during fractionation by AFFF. This is important for applications in nanomedicine requiring high purity with respect to both the medium and the cluster size.[7,11,15]

To quantify the relationship between peak position (hydrodynamic size) and the cluster number n, we define a ratio $R = d_{p,n}/d_{p,n=1}$, where $d_{p,n}$ is the hydrodynamic diameter of GNCs with different n, and $d_{p,n=1}$ is the hydrodynamic diameter of the primary AuNP ($n = 1$). We observe a relatively consistent correlation between R and n for 10-GNCs and 30-GNCs, with $R \sim n^{0.46}$ (Figure 2c); this correlation appears to diverge somewhat with increasing cluster size, but as a first approximation all data are fit to a single curve. The scaling exponent obtained from this experimental fit is very close to the theoretical value predicted for a collinear structure[16] ($R \sim n^{0.47}$) and is slightly larger than the expected value for a close-packed structure[17] ($R \sim n^{0.41}$); packing structure calculations and characteristic scaling properties are discussed in the Supporting Information. AFM images are consistent with the FE-SEM results but provide a better three-dimensional visualization of the packing structure (Figure 2d). Moreover, the combined imaging results conclusively show that collinear and close-packed structures coexist when $n > 2$, and this most likely contributes to band broadening in the fractograms. As a result, the correlation derived from Figure 2c can be used, as a first approximation, to estimate the peak position for different types of GNCs having different associated n values.

An orthogonal comparison between AFFF and ES-DMA is both beneficial and informative, as the latter technique has a demonstrated ability to detect and resolve multiple particle populations with single-nanometer-scale resolution,[6,18] albeit in aerosolized form. Figure 3a shows particle size distributions measured by ES-DMA for the same ammonium acetate-conditioned AuNP suspensions previously analyzed by AFFF (refer to Figure 1a). The species of GNCs are identified using an analytical model derived in our previous work in combination with transmission electron microscopy measurements.[6,18] Comparing Figure 1a (AFFF) with Figure 3a (ES-DMA), although peak positions are

dx.doi.org/10.1021/ja203328j |J. Am. Chem. Soc. 2011, 133, 8884–8887

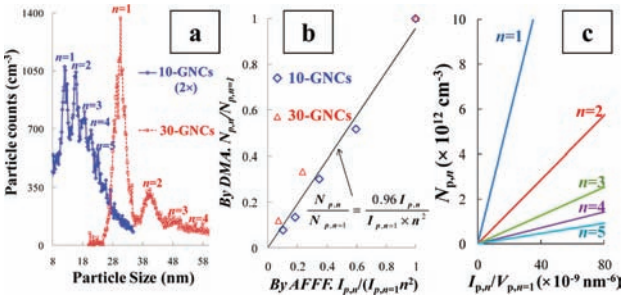

Figure 3. Comparison of AFFF and ES-DMA. (a) Particle size distributions from ES-DMA for the same samples analyzed by AFFF in Figure 1a. (b) $N_{p,n}/N_{p,n=1}$ (measured by ES-DMA) versus $I_{p,n}/I_{p,n=1}$ measured by AFFF (normalized by n^2). Diamonds, 10-GNCs; triangles, 30-GNCs. (c) Calculation of $N_{p,n}$ of GNCs from $I_{p,n}$ using eq 2. n ranges from 1 to 5.

not identical, at least five distinguishable peaks (from $n = 1$ to 5) are resolved by both methods for 10-GNCs. The results confirm that both AFFF and ES-DMA can be used to distinguish GNCs with different n when they fall into distinguishable sub-populations (i.e., when they do not generate a continuum of cluster sizes). The difference in the measured peak size between the ES-DMA and AFFF is attributed to differences in measurement conditions. We will defer a more detailed comparison of peak positions to the Supporting Information, but the two key factors are (1) the probability that collinear structures partially collapse as a result of the capillary forces generated during the ES-DMA aerosol formation and (2) actual differences between hydrodynamic size (i.e., in the wet state) and aerodynamic size (i.e., in the dry state).

ES-DMA is used to develop a quantitative approach to obtain the corresponding number concentration in solution from the measured scattering intensity during AFFF fractionation. Scattered intensity is measured at a scattering angle of 90° using a fiber-optic-based MALS detector ($\lambda = 632$ nm). For spherical nanoscale particles in the Rayleigh size regime, the angle-dependent scattering intensity is proportional to the number concentration of particles, $N_{p,n}$, times the volume-squared for an individual particle. Hence, as a first approximation, the scattered intensity of GNCs, $I_{p,n}$, should be proportional to $N_{p,n}$ times n^2,

$$I_{p,n} \sim N_{p,n}\left(\frac{V_{p,n}}{V_{p,n=1}}\right)^2 V_{p,n=1}{}^2 = N_{p,n}n^2V_{p,n=1}{}^2 \qquad (1)$$

where $V_{p,n}$ is the volume of GNCs having n primary particles per cluster, and $V_{p,n=1}$ is the volume of a singlet AuNP. Assuming the primary AuNP is spherical, $V_{p,n=1}$ will be equal to $\pi\, d_{p0}{}^3/6$, where d_{p0} is the nominal diameter of the singlet AuNP. By normalization, eq 1 becomes $N_{p,n}/N_{p,n=1} \sim I_{p,n}/(I_{p,n=1}n^2)$, where $I_{p,n=1}$ and $N_{p,n=1}$ are $I_{p,n}$ and $N_{p,n}$ of singlet AuNPs, respectively. As shown in Figure 3b, after fitting the corresponding $I_{p,n}$ for different values of n, a linear correlation between the relative number concentration ($N_{p,n}/N_{p,n=1}$) measured by ES-DMA and the relative scattered intensity ($I_{p,n}/I_{p,n=1}$) measured by AFFF is observed. The result of Figure 3b confirms that eq 1 is valid and can be used to obtain the composition of particle clusters in the native liquid phase (i.e., the degree of aggregation)[6] via an in situ AFFF analysis. Details for calculating $N_{p,n}$ are described in the Supporting Information.

In order to quantify the absolute GNC number concentration using the scattered intensity from the MALS detector, eq 2 is derived on the basis of the established correlation of eq 1,

$$N_{p,n} = N_{p,n=1,30nm}\frac{I_{p,n}V_{p,n=1,30nm}{}^2}{I_{p,n=1,30nm}n^2V_{p,n=1}{}^2} \qquad (2)$$

where $N_{p,n=1,30nm}$, $V_{p,n=1,30nm}$, and $I_{p,n=1,30nm}$ are the $N_{p,n}$, $V_{p,n}$, and $I_{p,n}$, respectively, for singlet AuNPs with $d_{p0} = 30$ nm. Figure 3c shows the calculation results using eq 2. We use $N_{p,n=1,30nm} = 2 \times 10^{10}$ cm^{-3} based on the information provided by the AuNP distributor and considering a 10× dilution, and the corresponding scattered intensity $I_{p,n=1,30nm} = 0.014$. Clearly, a linear correlation with a slope of $1/n^2$ is observed, implying that, for the same number concentration, GNCs with a larger n will show a higher scattered intensity. Hence, a better sensitivity for the detection of GNCs with larger n is expected for AFFF compared with ES-DMA, a number-density-based measurement.

In conclusion, simultaneous fractionation and quantitative characterization of GNCs was achieved using AFFF and validated using in situ UV−vis spectroscopy and ex situ FE-SEM and AFM. ES-DMA provided orthogonal information used to convert the intensity-based distributions obtained by AFFF into number concentrations. GNCs with different cluster numbers were successfully separated into enriched bands from the native mixture and then characterized under relevant fluid conditions. The experimental results presented here demonstrate proof of concept for an in situ AFFF-based approach that can potentially be used as a preparatory method to obtain highly enriched size-specific GNCs with a high-quality value.

■ ASSOCIATED CONTENT

Supporting Information. Materials information, instrumentation and methodology, calculation of size distributions from AFFF, calculation of cluster packing structures, additional FE-SEM and AFM images, and calculation of GNC number concentration from ES-DMA. This material is available free of charge via the Internet at http://pubs.acs.org.

■ AUTHOR INFORMATION

Corresponding Author
vince.hackley@nist.gov

■ ACKNOWLEDGMENT

The authors thank Robert Cook, Robert MacCuspie, Wolfgang Haller, Sang-Min Lee, and Rebecca Zangmeister at NIST for internal review and discussions.

■ REFERENCES

(1) Chak, C. P.; Xuan, S. H.; Mendes, P. M.; Yu, J. C.; Cheng, C. H. K.; Leung, K. C. F. *ACS Nano* **2009**, *3*, 2129–2138.
(2) Chen, G.; Wang, Y.; Tan, L. H.; Yang, M. X.; Tan, L. S.; Chen, Y.; Chen, H. Y. *J. Am. Chem. Soc.* **2009**, *131*, 4218–4219.
(3) Chen, G.; Wang, Y.; Yang, M. X.; Xu, J.; Goh, S. J.; Pan, M.; Chen, H. Y. *J. Am. Chem. Soc.* **2010**, *132*, 3644–3645.
(4) Jin, R. C. *Angew. Chem. Int. Ed.* **2010**, *49*, 2826–2829.
(5) Kim, J. Y.; Lee, J. S. *Nano Lett.* **2009**, *9*, 4564–4569.
(6) Tsai, D. H.; Pease, L. F.; Zangmeister, R. A.; Tarlov, M. J.; Zachariah, M. R. *Langmuir* **2009**, *25*, 140–146.
(7) Dobrovolskaia, M. A.; Patri, A. K.; Zheng, J. W.; Clogston, J. D.; Ayub, N.; Aggarwal, P.; Neun, B. W.; Hall, J. B.; Mcneil, S. E. *Nanomed. Nanotechnol. Biol. Med.* **2009**, *5*, 106–117.

(8) Keene, A. M.; Tyner, K. M. *J. Nanopart. Res.* **2011**, DOI: 10.1007/s11051-011-0268-4.
(9) Hall, J. B.; Dobrovolskaia, M. A.; Patri, A. K.; McNeil, S. E. *Nanomedicine* **2007**, *2*, 789–803.
(10) Zook, J. M.; MacCuspie, R. I.; Locascio, L. E.; Halter, M. D.; Elliott, J. T. *Nanotoxicology* **2010**, DOI: 10.3109/17435390.2010.536615.
(11) Tsai, D. H.; Delrio, F. W.; Keene, A. M.; Tyner, K. M.; MacCuspie, R. I.; Cho, T. J.; Zachariah, M. R.; Hackley, V. A. *Langmuir* **2011**, *27*, 2464–2477.
(12) Cho, T. J.; Hackley, V. A. *Anal. Bioanal. Chem.* **2010**, *398*, 2003–2018.
(13) Jana, N. R.; Gearheart, L.; Murphy, C. J. *Adv. Mater.* **2001**, *13*, 1389–1393.
(14) Allen, T. . In *Particle Size Measurement*, 3rd ed.; Chapman and Hall: London, 1981.
(15) Tsai, D. H.; Delrio, F. W.; MacCuspie, R. I.; Cho, T. J.; Zachariah, M. R.; Hackley, V. A. *Langmuir* **2010**, *26*, 10325–10333.
(16) Brenner, H. *Int. J. Multiphase Flow* **1974**, *1*, 195.
(17) Hoffmann, M.; Wagner, C. S.; Harnau, L.; Wittemann, A. *ACS Nano* **2009**, *3*, 3326–3334.
(18) Pease, L. F.; Tsai, D. H.; Hertz, J. L.; Zangmeister, R. A.; Zachariah, M. R.; Tarlov, M. J. *Langmuir* **2010**, *26*, 11384–11390.